Ab Initio Calculation of the Electronic Structure and Optical Properties of Diamond Using the Discrete Variational Method*

G. S. Painter
Metals and Ceramics Division, Oak Ridge National Laboratory, Oak Ridge, Tennessee 37830

and

D. E. Ellis† and A. R. Lubinsky
Physics Department, Northwestern University, Evanston, Illinois 60201

(Received 26 April 1971)

The electronic band structure, charge density, and optical properties of diamond have been calculated using the discrete variational method in an *ab initio* approach with an LCAO Bloch basis set. This technique avoids most of the difficulties encountered with evaluation of the matrix elements of the Hamiltonian, and allows inclusion of the nonspherical terms in the potential. A comparative study of the relative effects of muffin-tin averaging and scaling the $\rho^{1/3}$ statistical exchange reveals the large sensitivity of the energy bands to spherical averaging of the potential. For example, in diamond we find that neglect of the nonspherical potential terms shifts the indirect band gap by 5 times the change produced by scaling the exchange between Kohn-Sham and full Slater values. This demonstrates the inadequacy of the muffin-tin approximation for use in quantitative *ab initio* calculations. A comparison of the energy and location in the Brillouin zone of the indirect transition threshold indicates excellent agreement with experiment for an exchange scaling close to that determined by the X_α method. The conventional energy-level ordering is found, as opposed to that obtained in recent pseudopotential calculations. An analysis of the interband density of states reveals that this approach gives good agreement with the available optical data for diamond.

I. INTRODUCTION

There has been great interest in diamond from both experimental and theoretical viewpoints for some time. Recently, several band-structure calculations[1-4] have been published, based on different techniques, that give rather disparate descriptions of the energy bands in diamond; in particular, the pseudopotential calculations compare poorly with first-principles work. Consequently, there still exist some discrepancies between the theoretical situation and observed optical properties. This work represents an effort to resolve some of the questions concerning the band structure and optical properties of diamond, in view of the continued interest in this system. A previous application[5] of the method used in this work to the covalent crystal graphite met with considerable success in an *ab initio* approach to correlating the band structure with the observed optical properties. It would then be natural to suppose that this procedure could be applied to study the same atoms in the diamond crystal structure, with equally valid results. Diamond is rather the "classic" model of the covalent crystal, and this work is a first step towards more complete investigations to follow, not only on the one-electron properties, but also with regard to the cohesive energy of the various crystallographic phases of carbon.

The recent calculation by Hemstreet, Fong, and Cohen,[3] based on a nonlocal empirical pseudopotential model (referred to here as NEPM), yielded $\epsilon_2(\omega)$, in good agreement with experiment for the position of the main peak for type-I diamond, but the order of the levels is significantly changed from what has been obtained in first-principles band-structure calculations.[1,4] From the shifts of $\Gamma_{2'}$ relative to Γ_{15} observed in Sn, Ge, and Si, it seems natural to expect the lowest excited state at the zone center to be of Γ_{15} symmetry, not $\Gamma_{2'}$ as obtained in the NEPM. In this paper, we shall show that the results obtained from an *ab initio* calculation also lead to a satisfactory explanation of the optical properties, and yet remain within the conventional concept of the level ordering. This picture is further supported by the recent LCAO calculation of Chaney *et al.*,[4] which was, however, concerned primarily with the method involved, and was not used to extract the optical properties as is done in this work. Our main interest here is not so much concerned with the success of a particular computational method as with the fact that a completely *ab initio* calculation, without any *a priori* knowledge of either the energy bands or the experimental optical properties, gives results which agree very well with experimental data. To elaborate on our terminology, *ab initio* means here that a one-electron model Hamiltonian is set up, using nonspherical Coulomb potential and charge densities constructed by an *ad hoc* superposition of the free-atom quantities and employing the Slater exchange approximation.[6] The eigenvalue problem is then solved by a linear varia-

tion procedure in a selected basis set. In principle, the crystalline charge density and potential may be obtained, and the entire process iterated to achieve a self-consistent model.

After discussing the one-electron model Hamiltonian used in this calculation, we briefly review the discrete variational method (DVM)[7] as applied to the energy-band problem. In Sec. IV, results are presented for the application of the DVM to diamond. General features of the energy-band structure are related to the structure observed in the optical reflectivity, and the bonding properties of diamond are extracted from an analysis of the eigenfunctions. The crystal charge density, as calculated from the occupied orbitals, is next compared with the density resulting from overlapping carbon atoms. The relative sensitivity of the energy bands to details of the crystal potential is revealed through a study of exchange and muffin-tin averaging, which demonstrates the inadequacy of the muffin-tin model for a quantitative *ab initio* treatment of nonmetals and compounds with large nonspherical terms in the potential. We then consider the changes in band structure expected in a self-consistent model, and discuss the calculation of $\vec{k}$-dependent oscillator strengths. The interband density of states is related to the observed optical reflectivity and compared with the results of pseudopotential calculations. In Sec. V, a discussion is presented of the adequacy of the *ab initio* one-electron treatment for this case, as contrasted with that for an ionic system, and the relative merits of this approach are compared with those of semiempirical methods.

II. ONE-ELECTRON MODEL

The successful application of the independent particle approximation to crystalline solids has been based on a plausible effective one-electron model Hamiltonian. The difficulties of directly solving the Hartree-Fock equations for the solid have been circumvented by the introduction of the free-electron $\rho^{1/3}$ local exchange approximation,[6] which apparently constitutes a better approach to calculating one-electron transitions than using the Hartree-Fock eigenvalues directly. The Hartree-Fock-Slater (HFS) Hamiltonian can be written in Hartree's atomic units as

$$H^s(\vec{r}) = -\nabla^2/2 + V_c(\vec{r}) + V_x^s(\vec{r}) , \tag{1}$$

where $V_c(\vec{r})$ represents the effective Coulomb potential for an electron in the crystal and $V_x^s(\vec{r})$ is a local potential approximation to account for the exchange-correlation effects on the electron of spin s. A quite useful and commonly applied *ad hoc* procedure for forming the effective Coulomb potential is that of superimposing free-atomic (or ionic) Coulomb potentials from the atoms (or ions) on the crystal lattice sites (with suitable summation-truncation methods for point ion contributions). We have

$$V_c(\vec{r}) = \sum_{\eta, i} V_i(\vec{r} - \vec{R}_\eta - \vec{\mu}_i) , \tag{2}$$

where the sum on i is over all atoms in the unit cell defined by lattice vector $\vec{R}_\eta$. This construction technique will be referred to as the free-atom superposition model. The atomic charge densities are used in the same way to form the local crystal charge density, and in the Slater $\rho^{1/3}$ exchange approximation

$$V_x^s(\vec{r}) = -3\alpha[(3/4\pi)\sum_{\eta, i} \rho_i^s(\vec{r} - \vec{R}_\eta - \vec{\mu}_i)]^{1/3} , \tag{3}$$

where α is an exchange scaling parameter.[8] For the nonmagnetic solid, the total crystal charge density ρ_x is related to the density of spin s via $\rho_x = 2\rho_x^s$.

This procedure is used to construct the effective crystal potential used in the calculations reported here. Further approximations, such as forming the muffin-tin spherical average, are not necessary for the computational technique used in this study. In the muffin-tin model, the solutions inside each sphere can be written in separable form, and the radial solutions obtained by efficient numerical integration of the radial part of the Schrödinger equation, allowing exact solutions to the model Hamiltonian within each region. The popular first-principles APW and Green's-function (KKR) methods[9] derive their efficiency through this potential model, which is an adequate representation of the crystal potential in most metals. However, the nonspherical terms for nonmetals and compounds are not negligible and, as will be illustrated in this work, render the muffin-tin model inadequate for carrying out *ab initio* calculations of properties to be used for quantitative comparison with experiment. A further approximation often introduced to facilitate calculation of matrix elements in the superposition model is that of interchanging the orders of the summation and one-third power operations on the charge density in computing the statistical exchange.[10] Our studies on the potential construction in diamond indicate that the resulting potential differs nonuniformly from that constructed according to Eq. (3). Except for its use as a first step in a self-consistent calculation, summing atomic exchange potentials can be expected to introduce errors into the energy bands for crystals with asymmetric charge density.

Much effort has been devoted recently to finding methods best suited for treating the problems associated with the nonspherical terms in the first-principles Hamiltonian.[11-13] Considerable use has been made of various pseudopotential, OPW, and

LCAO parametrization schemes[14]; however, our interest is concentrated on the methods that can be used in an *ab initio* sense. The KKR and APW methods are specifically adapted to exploit the muffin-tin form of the potential, and although the influence of the nonspherical potential terms can be studied as a perturbation, this is seldom carried out due to computational difficulties. In the warped muffin-tin adaptation[12] of the APW method, the interatomic nonspherical terms are treated by expansion in a Fourier series. More complicated techniques involve expanding the terms inside the spheres in spherical harmonics[13]; however, this modification drastically increases the basic computation time and is usually used only at high symmetry points. The OPW method[10,15] is widely used for treating crystalline compounds; however, the procedure is not particularly advantageous for applications to compounds in which the valence electrons occupy orbitals with maxima rather far inside the atom, e.g., the $3d$ electrons. Poor convergence can also result for levels of symmetry not present as core states. Another approach which is useful for compounds, the LCAO method, [16] is founded on the hypothesis that much of the atomic character is maintained in the solid. This method, based on the linear variational formulation, is a convenient and adequate technique for treating the energy-band problem for covalent crystals such as diamond, and forms our choice for the calculation described in this paper.

III. DISCRETE VARIATIONAL METHOD

The DVM is based on a linear variational approach to the crystal energy-band problem. First, we will briefly review the formulation of this procedure and then illustrate the advantages that are obtained with the DVM when an LCAO Bloch basis set is used. In the linear variational procedure, we seek eigenfunctions as linear combinations of a predetermined basis set, which, for the energy band problem, is composed of Bloch functions $\{\chi_j(\vec{k},\vec{r})\}$. We have the following:

$$\psi_i(\vec{k},\vec{r}) = \sum_j \chi_j(\vec{k},\vec{r}) C_{ji}(\vec{k}) \ . \tag{4}$$

The coefficients are determined by minimizing expectation values of the Hamiltonian, defined as weighted discrete sums, with respect to variations of the coefficients $\{C_{ji}\}$:

$$\Delta_{ij} = \langle\psi_i|(H-E)|\psi_j\rangle = \sum_{m,n} C^*_{ni}\langle\chi_n|(H-E)|\chi_m\rangle C_{mj} \ . \tag{5}$$

Requiring $\partial\Delta_{ij}/\partial C_{pq}$ to vanish gives a set of N simultaneous complex equations for the coefficients in a basis set of N functions. In matrix form, the problem is expressed as

$$\underline{\hat{H}}(\vec{k})\underline{\hat{C}}(\vec{k}) = \underline{\hat{\epsilon}}(\vec{k})\underline{\hat{S}}(\vec{k})\underline{\hat{C}}(\vec{k}) \ , \tag{6}$$

where

$$H_{ij} = \langle\chi_i|H|\chi_j\rangle \ , \quad S_{ij} = \langle\chi_i|\chi_j\rangle \ . \tag{7}$$

Here the angular brackets denote a weighted sample mean, $\langle F\rangle = \sum_p w_p F(\vec{r}_p)$, as described previously.[7] This secular problem is solved by standard matrix diagonalization procedures. We solve this set of equations for each $\vec{k}$ of interest, and the resulting set of diagonal elements of $\hat{\epsilon}(\vec{k})$, displayed as a function of $\vec{k}$, forms the energy-band structure of the crystal. The DVM can be used directly to solve the eigenvalue equations, thereby avoiding the major problem with the conventional variational procedure—the evaluation of integral matrix elements of the Hamiltonian for a general crystal potential. Expressing the Bloch orbital in terms of translationally invariant functions u_j, we have

$$\chi_j(\vec{k},\vec{r}) = M^{-1/2} e^{i\vec{k}\cdot\vec{r}} u_j(\vec{k},\vec{r}) \ , \tag{8}$$

where M is the number of unit cells in the repeating volume of the crystal. In the DVM, we make use of the translational invariance of the Hamiltonian and the functions u_j to reduce the matrix elements to averages over a single unit cell and evaluate these numerically. For a potential term in the Hamiltonian we have, for example,

$$V_{ij}(\vec{k}) = \langle\chi_i|V|\chi_j\rangle = \sum_{m=1}^{N} w(\vec{r}_m) u_i^*(\vec{k},\vec{r}_m) V(\vec{r}_m) u_j(\vec{k},\vec{r}_m) \ , \tag{9}$$

where the sample points are confined to a single unit cell, and $w(\vec{r})$ is the weight function corresponding to the particular point density function used to generate the sample points.

The DVM can be used with a wide variety of basis functions. To describe systems with tightly bound electrons we may choose Bloch sums of atomiclike functions (e.g., Slater-type orbitals). In this case we have

$$\chi_j(\vec{k},\vec{r}) = M^{-1/2} \sum_{\nu=1}^{M} e^{i\vec{k}\cdot\vec{R}_\nu} a_j(\vec{r}-\vec{R}_\nu-\vec{\mu}_j) \ , \tag{10}$$

where

$$a_j(\vec{r}) = x^l y^m z^n \gamma^p e^{-\beta r} \ , \tag{11}$$

with subscript j representing the orbital parameters (l,m,n,p,β). Basis set parameters used in this calculation are given in Table I. This basis is quite adequate for narrow-band covalent crystals, and recent work[4,5] shows that sufficient variational freedom can be incorporated into such a basis to approach a complete set over a reasonably wide energy range for covalent crystals of light atoms. Materials in which d bands play an important role are also treated without difficulty; band structure and related properties for cubic SiC and TiC will

TABLE I. Atomic STO basis functions used to construct Bloch orbitals on each carbon site.

$1s$	$e^{-8.335r}$
$1s'$	$e^{-5.4r}$
$2s$, $2px$, $2py$, $2pz$	$\begin{Bmatrix} r \\ x \\ y \\ z \end{Bmatrix} e^{-1.4r}$
$2p'x$, $2p'y$, $2p'z$	$\begin{Bmatrix} x \\ y \\ z \end{Bmatrix} e^{-2.642r}$
$3s$	$r^2 e^{-1.4r}$
$3px$, $3py$, $3pz$	$r\begin{Bmatrix} x \\ y \\ z \end{Bmatrix} e^{-2.642r}$

be presented in a subsequent article. The DVM is particularly well suited for handling the difficulties associated with the LCAO basis since the multicenter integral problem is avoided. In this approach, the matrix elements are formed by evaluating the basis functions $\{\chi_j(\vec{k}, \vec{r})\}$ directly over the integration grid, without any further decomposition into atomic constituents.

IV. RESULTS

A. Crystal Potential

One of the most attractive features of the DVM is the facility it offers for using crystal potentials of general unrestricted form, e.g., nonspherical potential terms can be included in the Hamiltonian. This is particularly important for diamond, in which the highly directional bonding charge distribution produces sizable nonspherical Coulomb and exchange potential terms. As an example of the great oversimplification of the muffin-tin model for such potentials, the superposition construction procedures described in Eqs. (2) and (3) were used to generate a crystal potential which was then compared with its muffin-tin average. The nonspherical potential was averaged into muffin-tin form by a direct (least-squares) fit to spherically symmetric polynomials inside touching carbon atom spheres. The potential over the volume outside the spheres was fit to a constant, thus yielding the expansion

$$V(r) = \sum_{i=1}^{9} c_i r^{i-2} e^{-1.3r}, \quad r \text{ inside carbon spheres}$$
$$= V_0, \quad r \text{ outside carbon spheres}. \tag{12}$$

TABLE II. Least-squares coefficients for spherical average potential.

C_1	−6.0016529
C_2	+2.2022760
C_3	−2.5019666
C_4	−2.0906299
C_5	−0.7672562
C_6	+0.3834775
C_7	+0.9946675
C_8	+0.7493132
C_9	−0.8279715
V_0	−0.8076969 a.u.

For reference, the coefficients c_i are listed in Table II. In Fig. 1 we present the crystal potential in diamond (exchange $\alpha = 0.76$) along various crystallographic directions from one of the carbon atoms, as generated by the superposition method, and compare with the resulting muffin-tin average potential. The magnitude of variations in the nonspherical potential is about 1.0 Ry, from the bond center in the unit cell to a point inverted through an atom site. This oscillation comprises a 35% variation about the muffin-tin value, and the deviation of the full potential at the bond center (noted R_s in Fig. 1) from the muffin-tin value exceeds 0.6 Ry. The energy-band structure is sufficiently sensitive to this averaging to cause a 16% reduction in the direct band gap at the Brillouin-zone center compared to the gap found with the complete potential. Even more conclusive demonstration of the inadequacy of the muffin-tin model with regard to meaningful calculations for diamond is found with the behavior of the indirect band gap. This is one of the most accurate experimentally determined features for diamond and the calculated value is found to be in excellent agreement when the full nonspherical potential is used; however, in the muffin-tin case the value is reduced by 30%.

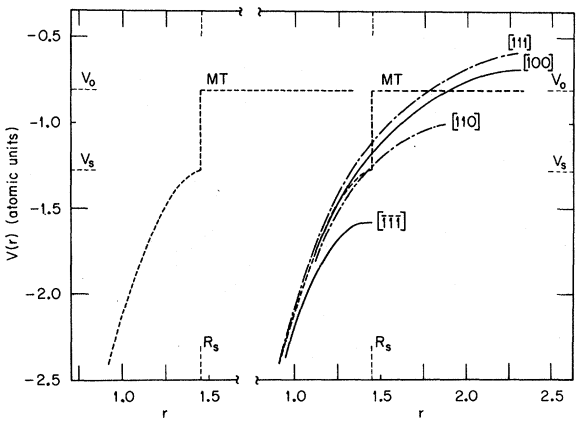

FIG. 1. Comparison of the nonspherical crystal potential plotted along various crystallographic directions with its muffin-tin average (dashed curve). With the origin at one atom, the other atom occupies the position $-2R_s/\sqrt{3}$ (1, 1, 1) in the unit cell, where R_s denotes the muffin-tin radius. Lattice constant $a = 6.7406$ a.u.

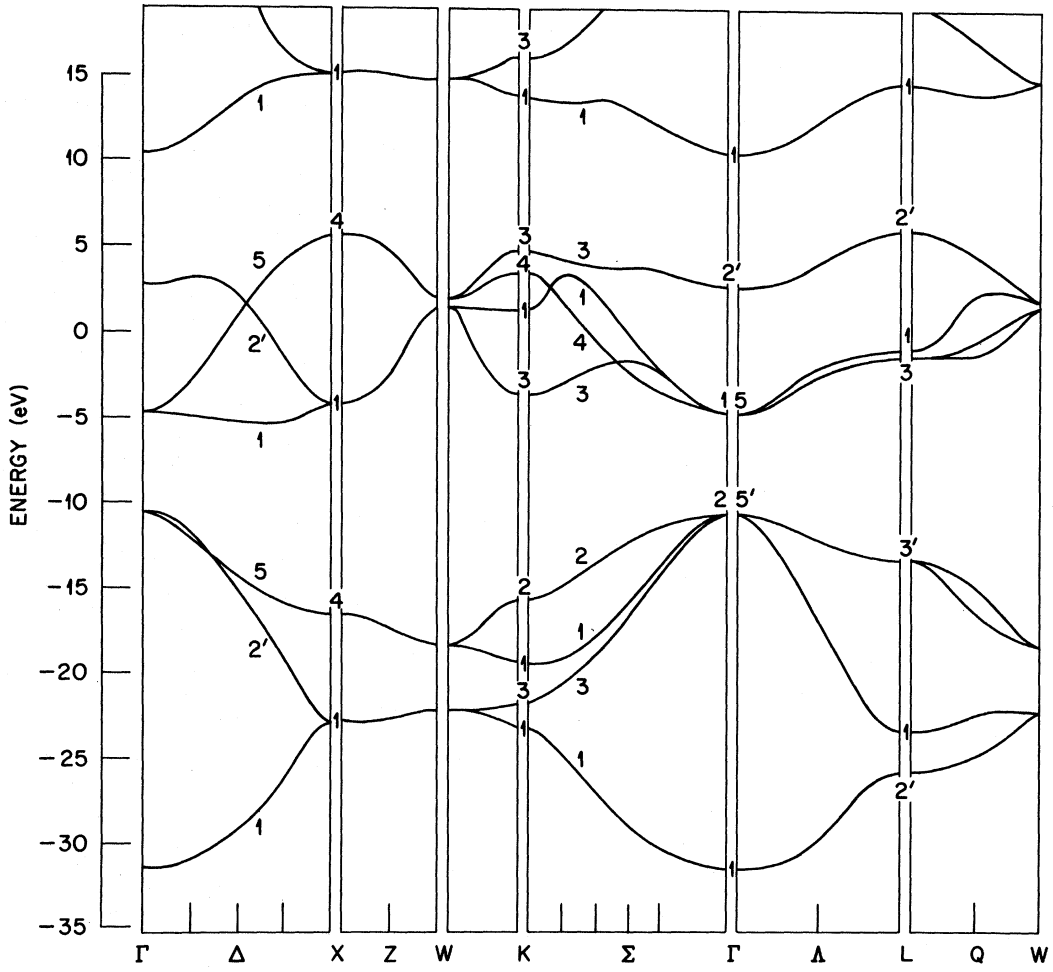

FIG. 2. Energy-band structure of diamond calculated using the DVM with X_α exchange scaling $\alpha = 0.76$. Not appearing are the carbon core states at ~ -278.6 eV.

B. Energy-Band Structure

The energy bands calculated with a full nonspherical potential for assumed neutral carbon atom configurations and an X_α value of exchange scaling ($\alpha = 0.76$) is given in Fig. 2. In general, our calculations show the material to be characterized by a fairly broad set of valence bands composed of carbon $2s$, $2p$ orbitals, with a relatively narrow (~10 eV) low-lying set of conduction bands composed predominantly of antibonding combinations of carbon $2s$, $2p$ states with a slight, but significant, admixture of carbon $3s$, $3p$ orbitals. The $3d$ carbon states contribute relatively little to this energy range. Convergence characteristics of the calculation are discussed further in the Appendix.

The narrow conduction bands, composed of atomiclike wave functions, are in marked distinction to the free electronlike bands obtained in the NEPM calculation, and this is certainly one significant cause of the differences in the optical properties calculated by these two methods. Another interesting general feature of the band structure is the existence of a second band gap separating the lower set of conduction bands from a set of higher-energy excited levels. Transitions from the valence bands to these higher states involve energies in excess of 20 eV. However, this still overlaps the upper part of the energy range for allowed transitions to the lower-lying set of conduction bands; thus the existence of the second gap would be difficult to verify experimentally—there would be no second threshold and the transition energies of interest are large. The only well-established transition in diamond seems to be that associated with the threshold for indirect transitions, 5.47 eV,[17] between the zone center and the conduction band minimum which is found at $(0.78 \pm 0.02, 0, 0)$ from neutron diffraction work.[18] Our calculations, using the full potential, give an energy separation of 5.40 eV between

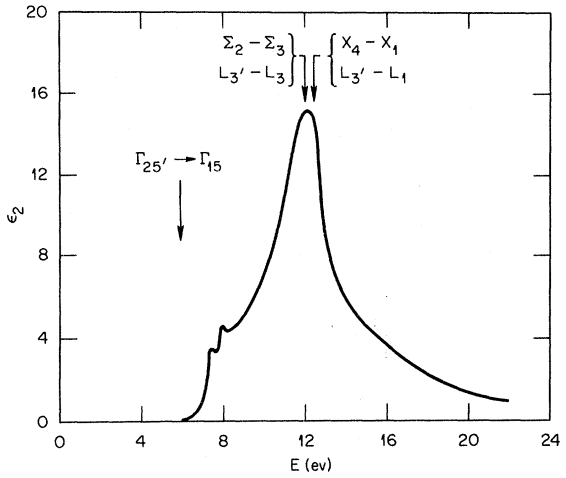

FIG. 3. Experimental imaginary part of the complex dielectric function for type-IIa diamond from the paper of Roberts and Walker (Ref. 19). Positions of important structure producing transitions derived from the band structure of Fig. 2 are indicated.

the valence band maximum at Γ and the conduction band minimum at ~(0.7, 0, 0). The nonspherical terms are crucial to accurately calculating this detail of the band structure.

The paper by Roberts and Walker[19] gives a good summary of the development of the optical investigations of diamond. The main feature of the experimental optical reflectivity is the existence of a strong peak at about 12.2 eV. An examination of the band structure shows that agreement with this observed peak in the structure is predicted originating from the singular critical transition X_4-X_1 at ~12.5 eV and the transitions $L_{3'}$-L_3 and $L_{3'}$-L_1 at 12.0 and 12.5 eV, respectively. The growth of the main peak appears to be associated with transitions originating at the zone center (direct threshold $\Gamma_{25'}$-Γ_{15} at 6.0 eV) and extending along Λ to the critical points at L (12.0 and 12.5 eV) and along $\Sigma(\Sigma_2$-$\Sigma_3)$ to the K point transition, 12.1 eV. Only a detailed calculation of the imaginary part of the dielectric function $\epsilon_2(\omega)$ would fix the position of our main peak; however, results are presented in Sec. IV E of a calculation of the energy-weighted interband density of states, which relates to the experimentally determined optical properties. Qualitatively, it is of interest to note from the band structure that the main peak in the experimental $\epsilon_2(\omega)$ curve (Fig. 3) is bounded on the low-energy side (12.0 eV) by the transitions $L_{3'}$-L_3, and transitions between the upper valence and lower conduction bands Σ_2, Σ_3 which are quite parallel away from Γ. On the high-energy side (12.5 eV) the peak is bounded by $X_4 - X_1$ and $L_{3'} - L_1$. In Sec. IV E, we will present a more quantitative comparison with experiment and other works. The band structure of Fig. 2 was used in all calculations of properties discussed subsequently.

C. Wave Functions and Crystal Charge Density

The well-known picture of the cohesive properties of diamond[20] is based on the formation of strongly bonding covalent orbitals in the crystal. From our energy-band calculations, the wave functions are easily reconstructed from the solution coefficient matrices [Eq. (4)]. The occupied bonding crystal wave functions at the zone center for diamond are plotted along a [111] line connecting nearest-neighbor carbon sites in Figs. 4(a) and 4(b): State Γ_1 is a low-lying (−1.16 a.u.) bonding combination of carbon 2s Bloch orbitals, while the orbital for $\Gamma_{25'}$ is one representative of the set of d-like bonding combinations of carbon 2p Bloch states for this triply degenerate level. The higher-energy p-like Γ_{15} antibonding combination of carbon 2p Bloch orbitals is shown in Fig. 4(c) and is distinguished from the $\Gamma_{25'}$ state by having a node midway along the carbon-carbon bond.

The occupied bonding states give a charge increase in the bond region in excess of that obtained by simply superimposing free-atom charge densities. The charge density calculated from the crystal eigenfunctions is shown in Fig. 5(a). This crystal density is calculated as

$$\rho_x(\vec{r}) = -\sum_i \sum_{\vec{k}} |\psi_i(\vec{k}, \vec{r})|^2 w(\vec{k}) , \qquad (13)$$

where i sums over occupied bands, $w(\vec{k})$ is an appropriate k-integration weight function for summing $\vec{k}$ over the Brillouin zone, and $\{\psi_i(\vec{k}, \vec{r})\}$ represents the set of eigenfunctions of the Bloch Hamiltonian. The amount of charge transfer in the crystal predicted by our calculations is given in Fig. 5(b), where we compare the crystal charge density ρ_x with the superimposed density of overlapping neutral carbon atoms ρ_{SD} in the difference density $\rho_x - \rho_{SD}$. The atomic density is that obtained from a version of Herman and Skillman's HFS program for free-atom calculations.[21] Charge is built up in the nearest-neighbor interatomic region by depleting charge in the volume away from the bond region. This charge density increase is a consequence of the formation of the bonding Γ_1 and $\Gamma_{25'}$ states which are hybridized along the bond. There is also a slight contraction of the carbon atom (not shown), which becomes a bit difficult to distinguish from the contribution to the difference density due to different basis sets being used in the crystal and atomic calculations. The relatively small magnitude of the difference density $\rho_x - \rho_{SD}$ in the unit cell indicates that there will be no great changes in the energy-band structure obtained from a first iteration to self-consistency. The crystal charge density calculated with 32 wave vectors in the Brillouin

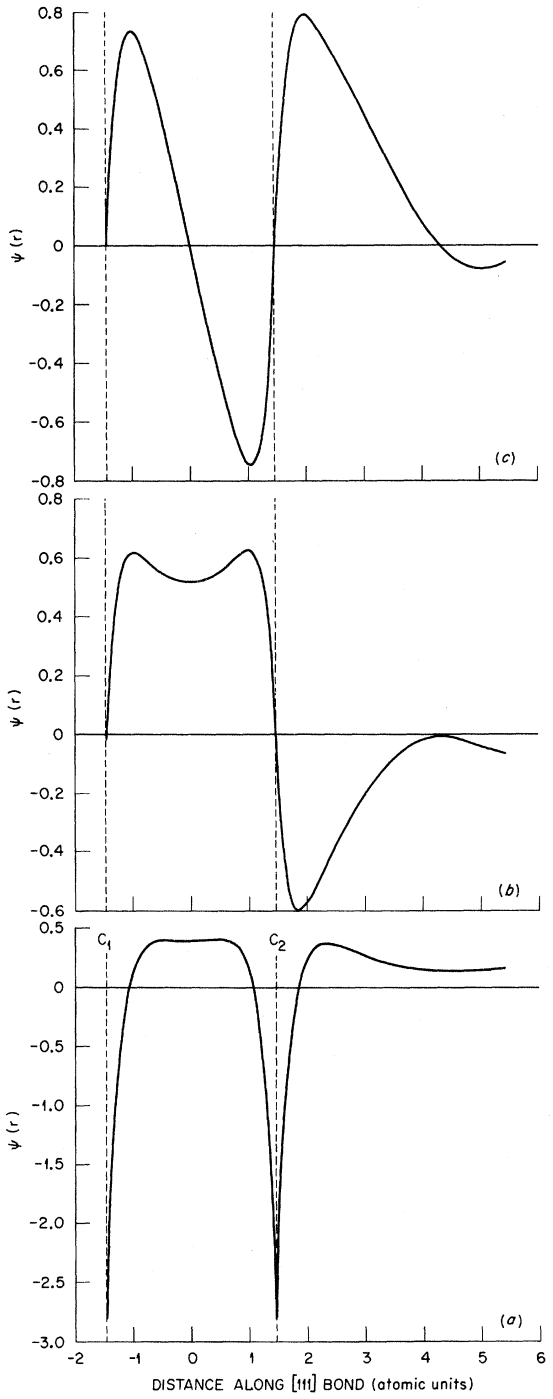

FIG. 4. Crystal wave functions at point Γ in the Brillouin zone. Occupied orbitals of s-like (Γ_1) and d-like ($\Gamma_{25'}$) symmetry appear in (a) and (b), respectively, while a p-like (Γ_{15}) excited wave function is plotted in (c).

zone changes only slightly upon extending the $\vec{k}$ integration to include 256 wave vectors.

D. Exchange Scaling, Muffin-Tin Effects, and Self-Consistency

A previous application of the DVM to the calculation of the band structure of graphite,[5] which is typically considered a covalent crystal, has revealed relative stability (within uniform shifts) of the overall band structure with respect to slight modifications of the crystal potential through scaling of the Slater $\rho^{1/3}$ exchange approximation. An application of the DVM to a calculation of the energy bands of the ionic system LiF (Ref. 22), however, revealed that the band structure for that system was very sensitive to variations in the potential. For example, the direct band gap at Γ varied by more than 35% for α in a range between 0.67 and 1.0, and this nonuniform band shift was explained in terms of differences in the character of the wave functions for the valence and conduction bands. In Fig. 6, some results of a similar study of exchange sensitivity in diamond are summarized by illustrating the variation of the direct and indirect transition thresholds and the valence bandwidth as functions of α (between Kohn-Sham[23] and full Slater values). From these variations (less than 6% and 4% for the gaps and valence bandwidth, respectively) the insensitivity of the band structure, with respect to exchange scaling, is evident. This behavior is typical of the covalent crystals treated hitherto, but contrasts distinctly with that observed in the ionic crystal LiF. Whereas in LiF the orbitals defining the band gap are characterized by compact valence states and diffuse conduction states, the diamond wave functions defining the direct gap at Γ are all well described by Bloch sums of carbon $2p$ orbitals, whose maxima occupy regions of about the same magnitude charge density. Thus, scaling the exchange part of the energy matrix elements has nearly the same effect on the valence and conduction band eigenvalues. In LiF, however, the conduction bands are so free-electron-like that they are not changed as much as the localized p-like valence band states; thus the band gap in LiF varies by more than 5 eV for the same α scaling shown in Fig. 6 (wherein the change is 0.35 eV). It is interesting to note from Fig. 6 that the indirect band gap for the X_α exchange[8] is in somewhat better agreement with the experimental value of 5.47 eV than that for full Slater exchange. From the results of this study, it is apparent that the effects of scaling the statistical exchange approximation are fairly small and play a minor role in determining the electronic structure and optical properties of diamond. On the other hand, the symmetry of the potential is a physical feature which is quite important in differentiating between the valence and conduction band states in covalent crystals, since the relevant wave functions generally belong to different symmetry species. This is demonstrated quite vividly in the case of diamond, where the direct band gap is reduced by ~16% when nonspherical potential terms are deleted from the Hamiltonian. Simi-

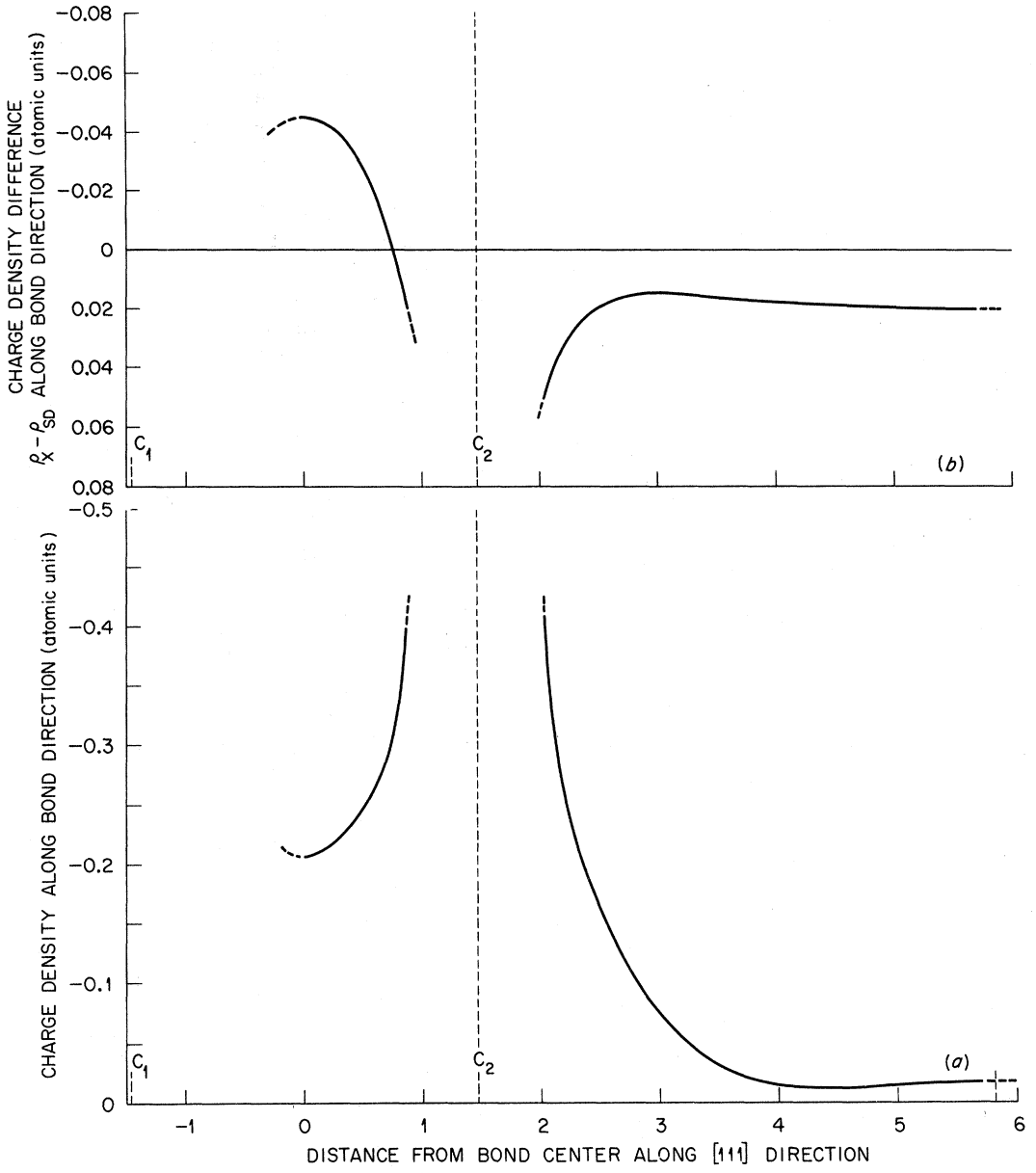

FIG. 5. (a) Crystal charge density ρ_x calculated from the occupied Bloch orbitals. (b) Charge transfer $\rho_x - \rho_{SD}$ along the (1, 1, 1) bond; ρ_{SD} is the superimposed free-atom density.

larly, the indirect gap is reduced by about 30% to a value (3.8 eV) which falls below the scale of Fig. 6. Thus, while *ab initio* computations within the muffin-tin model can be useful for obtaining the gross qualitative features of the energy bands for compounds characterized by large nonspherical potentials, a quantitative comparison with experiment can be expected to reveal sizable discrepancies. These discrepancies can be minimized by taking the constant potential term V_0 as an adjustable parameter[24]; however, this scheme is far less versatile for data fitting than many other empirical methods, e.g., pseudopotential and parametrized tight-binding schemes. Our interest lies primarily in developing an *ab initio* approach; in this sense the use of an exchange scaling parameter is considered a temporary expedient.

The agreement with experiment of the calculated indirect transition threshold that is obtained with the full crystal potential defined by the atomic superposition model affords another indication of the extent to which crystalline solids maintain the physical characteristics of the constituent atoms. The extent to which a self-consistent model would

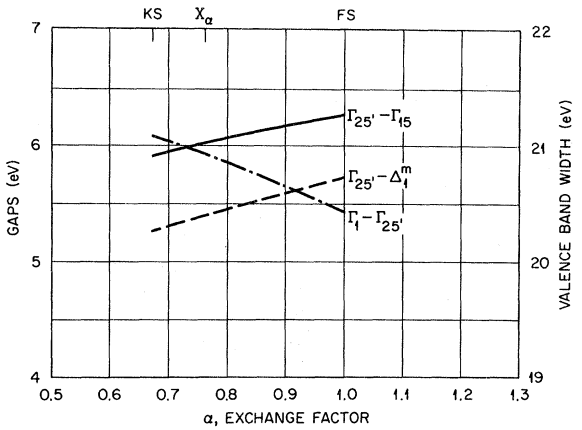

FIG. 6. Exchange variation of threshold band gaps and valence bandwidth. The illustrated gaps define the direct and indirect transition thresholds; $\Gamma_1-\Gamma_{25'}$ defines the valence bandwidth.

give different results depends, of course, upon our initial choice of potential. In systems with competing atomic configurations, for example $3d^{n-x}4s^x$, self-consistency effects are doubtlessly quite important. In carbon, the model potentials based on s^2p^2 or sp^3 configurations are not greatly different, and we estimate that, aside from uniform shifts, the level intervals may change by a few percent, i.e., of the same order as the choice of exchange parameter. This has been our experience in self-consistent molecular studies of simple hydrocarbons. A study is planned to see whether self-consistent bands merely lead to a slightly different "optimized exchange parameter," or whether significant differences arise.

E. Optical Properties

A least-squares fit to the valence and conduction bands was generated from the energy-band data calculated at 45 inequivalent wave vectors in the Brillouin zone. The fitting functions were symmetrized sums of plane waves, i.e.,

$$F_s(\vec{k}) = \sum_\nu e^{i\vec{k}\cdot\vec{R}_\nu} , \tag{14}$$

where the lattice vectors $\{\vec{R}_\nu\}^s$ comprise a set of vectors into which the sth transforms under cubic operations. The corresponding energy expression

$$\epsilon_j(\vec{k}) = \sum_{s=1}^{K} b_s^j F_s(\vec{k}) \tag{15}$$

is a Fourier representation of the energy in the jth band which has the proper symmetry in the Brillouin zone. In this work, we typically used $K=25$. Through irrational vector sampling[25] in the Brillouin zone, this fit of the bands was used to form histogram representations of the density of states in each band. We have

$$g_j(E) = \frac{2}{(2\pi)^3}\int d\vec{k}\,\delta(\epsilon_j(\vec{k}) - E) \tag{16}$$

in the form

$$\tilde{g}_j(E) = \frac{2}{N}\frac{1}{\Delta E}\sum_{i=1}^{N}\Delta_j(\vec{k}_i) , \tag{17}$$

where $\Delta_j(\vec{k}_i)$ is unity if $\epsilon_j(\vec{k}_i)$ is within an interval ΔE about E, zero otherwise, and the $\{\vec{k}_i\}$ are the sampling vectors. For our final calculations, we used $\Delta E = 0.01$ a.u. and N was tested in the range of 10 000 to 50 000. In Fig. 7 we plot the total band density of states (in states/a.u./cell), $D(E) = \sum_j \tilde{g}_j(E)$, in the energy range -1.2 to 0.2 a.u.

To compare with the experimental optical properties of diamond, we have calculated the energy-weighted interband joint density of states, to which $\epsilon_2(\omega)$ is proportional through the average interband strengths $\bar{f}_{ij}$. The imaginary part of the complex dielectric function $\epsilon_2(\omega)$ is given by[26]

$$\epsilon_2(\omega) = \frac{2e^2h^2}{m}\sum_{j,i}\frac{1}{(2\pi)^3}\int d\vec{k}\, f_{ij}(\vec{k})\,\frac{\delta(E_j - E_i - \hbar\omega)}{E_{ji}(\vec{k})} . \tag{18}$$

As a preliminary to accurate calculation of the dielectric function, it is useful to consider simplified forms of Eq. (18); for purposes of comparison with previous work a "constant matrix element" approximation is convenient. We have imposed the approximation that the interband oscillator strengths

$$f_{ij}(\vec{k}) \propto |\langle\vec{k}|\vec{p}|\vec{k}\rangle|^2/E_{ji}(\vec{k}) \tag{19}$$

do not vary with respect to wave vectors. In the histogram representation, we obtain the interband density of states

$$I_{ij}(E) = \frac{1}{(2\pi)^3}\int d\vec{k}\,\delta(E_{ji}(\vec{k}) - E) \tag{20}$$

in exactly the same way as for the ordinary density of states, except that we sample the energy differences $E_{ji}(\vec{k}) = E_j(\vec{k}) - E_i(\vec{k})$. We then form the quantities $I_{ij}(E)/E$, which determine the imaginary part of the complex dielectric function approximated by

$$\epsilon_2(\omega) = A\sum_{j,i}\bar{f}_{ij}I_{ij}(E)/E . \tag{21}$$

The densities $I_{ij}(E)/E$ have been obtained for the 16 valence-conduction band pairs which contribute to the structure of $\epsilon_2(\omega)$ below ~20 eV. Preliminary studies of the $\bar{f}_{ij}$ indicate that 4-5 transitions dominate the contributions to the structure of $\epsilon_2(\omega)$ from the direct threshold up to the neighborhood of the main peak in $\epsilon_2(\omega)$ at about 12 eV. At higher energies, contributions from other band pairs become important, and the validity of the constant matrix element approximation becomes particularly questionable. A detailed study of the quantities

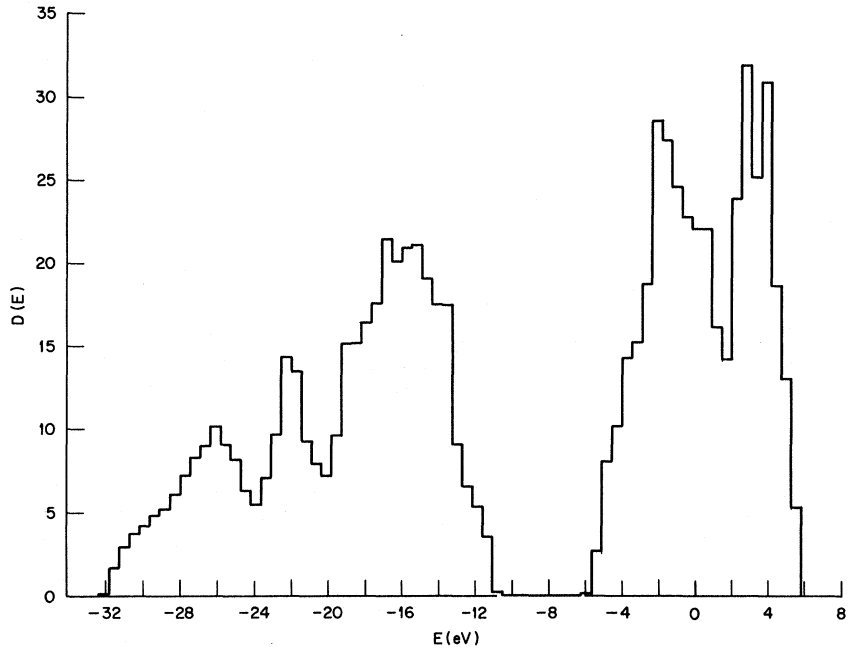

FIG. 7. Density of states calculated from a least-squares representation of the energy-band structure given in Fig. 2.

$f_{ij}(\vec{k})$ is in progress; for the present we give a more qualitative discussion of structure in the experimental data in terms of interband transitions between bands 4 and 5. In Fig. 8 we present results of a calculation of $I_{45}(E)/E$ using 50 000 wave vectors with an energy increment of 0.01 a.u. The general shape of this plot is very similar to the experimental $\epsilon_2(\omega)$ curve of Roberts and Walker[19] for type-IIa diamond reproduced in Fig. 3. From our calculations, a strong peak occurs at 11.8 ± 0.3 eV and there appears to be additional structure between 7.1 and 8.4 eV. Zone-center 4-5 transitions mark the direct threshold at about 6.0 eV. The excited level ordering at Γ for this calculation (Γ_{15} below $\Gamma_{2'}$) agrees with that of other first-principles calculations but differs from that determined in the pseudopotential model. An important consequence of the lowering of $\Gamma_{2'}$ below Γ_{15} in the pseudopotential work is a related lowering of $L_{2'}$ below L_3, while state L_1 is shifted to high energy. Hemstreet *et al.*[3] find a resulting M_1-type critical point transition $L_{3'}$-$L_{2'}$ producing a shoulder in $\epsilon_2(\omega)$ at 8.27 eV while we find $E_{4-5}(L) = 11.8$ eV. We find that the conduction band L_3 and L_1 levels lie very close to each other and determine the lowest-energy L-point transitions, which, being critical-point M_1-type excitations, will contribute strongly to the main peak in $\epsilon_2(\omega)$. On the other hand, $L_{2'}$ lies some 19.5 eV above $L_{3'}$. There is low-energy structure in the experimental $\epsilon_2(\omega)$ at 7.3 and 7.8 eV; our calculations place a shoulder in $I_{45}(E)/E$ at about 7.4 eV with some indications of weak structure coming at about 7.6 and 8.4 eV from the behavior of the bands near Γ. The position of the main peak in $I_{45}(E)/E$ is determined to be 11.8 eV compared to the 12.2-eV observed peak in $\epsilon_2(\omega)$ for type-IIa diamond which the theoretical perfect crystal model most closely approximates. Roberts and Walker also quote a peak in $\epsilon_2(\omega)$ of 12.0 eV for type-I diamond, with which the results of the NEPM are compared; however, we believe that the data for type IIa is more appropriate for the model crystal.

The predominant contributors to the main peak in $\epsilon_2(\omega)$ are predicted from our calculation to be the near-degenerate critical L-point transitions $L_{3'}$-L_1, $L_{3'}$-L_3, as well as the X_4-X_1, K_2-K_3, and Σ_2-Σ_3 transitions. Although the shape of the theoretically calculated $I_{45}(E)/E$ in the high-energy region agrees very well with the experimental dielectric function, there will be significant contributions to the theoretical $\epsilon_2(\omega)$ coming from 3-5 and 4-6 transitions in this range. The peaks which are found in the NEPM calculated $\epsilon_2(\omega)$ at 13.2 and 14.4 eV are a consequence of the lowering of the level $\Gamma_{2'}$ below Γ_{15}. Our bands do not display the characteristics that will result in this structure, nor are these peaks experimentally observed.

Concerning the temperature-dependent weak peak at 7.8 eV observed in the experimental optical data,[19] we observe a change in slope of the interband density of states at 7.5 ± 0.2 eV which appears to be due to critical points in the joint density superimposed upon nonsingular contributions. Although Hemstreet *et al.* tentatively identify this peak with the critical $L_{3'}$-$L_{2'}$ transition, their calculated energy is 8.27 eV. Further refinements of the work presented here will involve carrying the calculation to self-consistency and improving our *ab*

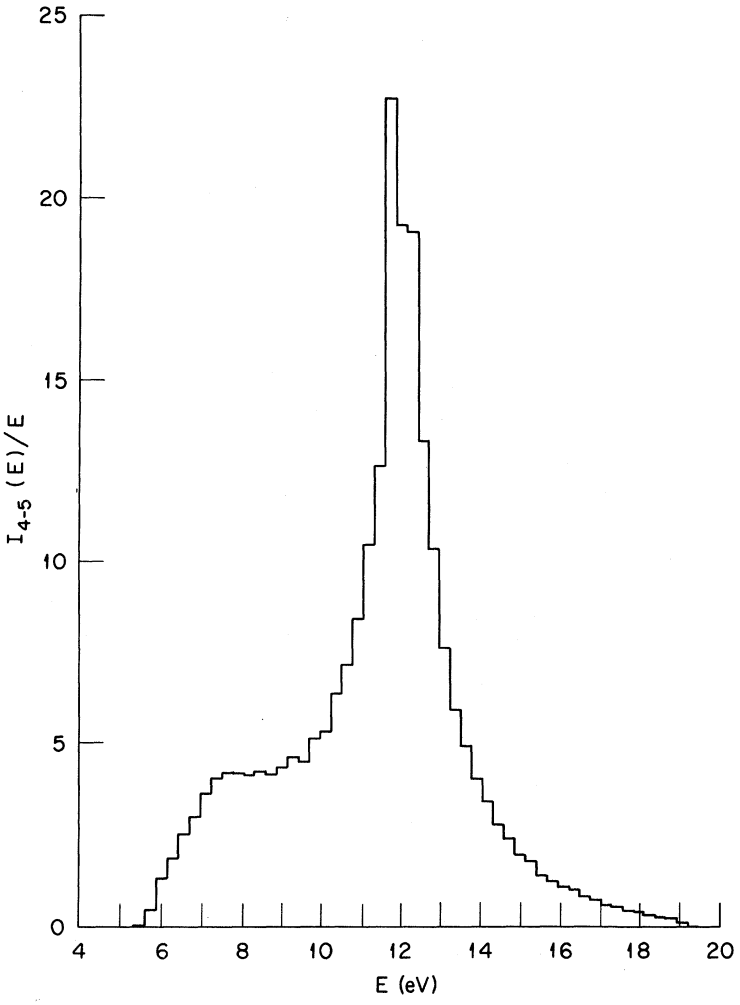

FIG. 8. Energy-weighted interband density of states for transitions between the highest valence and lowest conduction bands, as computed from a least-squares fit to the energy-band structure. This is to be compared with the experimental $\epsilon_2(\omega)$ curve of Roberts and Walker given in Fig. 3.

initio theoretically derived approximation to $\epsilon_2(\omega)$ by explicitly calculating the k dependence of the oscillator strengths $f_{ij}(\vec{k})$. Indications are that the contributions of additional interband transitions will shift the main peak of the $\epsilon_2(\omega)$ curve derived from the 4-5 transitions into closer agreement with that of the experimental $\epsilon_2(\omega)$. In particular, 4-6 transitions in the vicinity of the critical-point L_3,-L_1 transition at 12.5 eV will contribute significantly.

V. SUMMARY AND DISCUSSION

From the results of this calculation, it is evident that the *ab initio* variational approach to the energy-band problem for a covalent crystal works very well in the case of diamond, as in a previous application to graphite. The basic principles of the procedure involve constructing a full nonspherical crystal potential by superimposing free-atom charge densities and potentials and using the X_α exchange approximation, but without the approximation of spherical averaging. There are no difficulties in utilizing the potential in this form with the DVM, which again proves to be a rapidly convergent linear variational computation scheme. The quantitative aspects of the electronic band structure are rather insensitive to exchange scaling, with marginally better results in the one-electron properties for the X_α choice of α. On the other hand, the muffin-tin model is only qualitatively valid, leading to results which differ significantly from those obtained in cluding the nonspherical terms in the potential. From a comparison of the calculated physical properties with experiment, it appears that the relative magnitude of error introduced through muffin-tin averaging is large compared with the deficiencies inherent in the full one-electron model Hamiltonian itself. While calculations carried out in the muffin-tin model for covalent compounds can be used to provide the gross features of the energy bands, for a quantitative comparison with experiment, a full potential of the type discussed here should be used. From a comparison of the relative importance of the effects of spherical averaging and exchange scaling, we find the electronic structure to be much

more sensitive to the averaging than exchange scaling. This characteristic, with respect to exchange, contrasts with that of ionic systems and is understood in terms of the symmetry and spatial properties of the crystal wave functions. It is of interest to note that the X_α statistical exchange works well in the covalent systems, indicating that the correlation effects which have been omitted in the statistical exchange approximation largely cancel out in calculating one-electron transition energies.

The methods employed in this work to determine the interband density of states appear adequate to interpret the optical reflectivity within the conventional band picture for diamond. The zone-center excited Γ_{15} energy is found to lie lower than the $\Gamma_{2'}$ level, in contrast to the results of recent pseudopotential studies.[2,3] In addition to the X-point transition X_4-X_1, the L-point transitions $L_{3'}$-L_3 and $L_{3'}$-L_1 are found to be predominant contributors to the main peak in the reflectivity. We find the X_4-X_1 energy to be ~12.5 eV, while the critical L-point transitions occur at 12.0 and 12.5 eV.

The use of an LCAO basis within the DVM has been found to be adequate for converging the upper valence and lower conduction bands in diamond. A study of the spatial properties of the wave functions pertinent to these bands reveals that the Bloch states are quite localized near each nucleus. Thus plane-wave expansions are expected to be poorly convergent, perhaps explaining some of the problems encountered in OPW treatments of this crystal. The narrow bandwidth found for the lower set of conduction bands is in striking contrast to the free-electron-like bands obtained in this energy range in the pseudopotential calculations.[2,3] Further calculations are planned in order to obtain the imaginary part of the dielectric function more accurately so that a more exact comparison with experiment can be made. Progress is being made towards self-consistency in the DVM and further calculations will be carried out in this scheme.

ACKNOWLEDGMENTS

The authors wish to thank Professor W. C. Walker for providing a copy of the experimental $\epsilon_2(\omega)$ used in this paper. Computations were performed at the Oak Ridge National Laboratory Computation Center and at the Vogelback Computation Center of Northwestern University.

APPENDIX: CONVERGENCE PROPERTIES

To assure the accuracy of our calculations, with respect to the discrete point sampling, our final results were obtained with ~1300 integration points in the unit cell and a total of 26 Bloch basis functions, as given in Table I. In the energy range shown in the band structure of Fig. 2, the net uncertainty in energy is ascertained to be less than 0.4 eV, and for most levels the accuracy is much better.

TABLE III. Comparison of the energy eigenvalues of diamond at high symmetry points in the Brillouin zone. Energies (in eV) are measured with respect to the bottom of the valence band.

State	DVM	APW[a]	TB[b]
Γ_1	0.0	0.0	0.0
$\Gamma_{25'}$	19.6	19.6	19.2
Γ_{15}	25.6	25.4	24.9
$\Gamma_{2'}$	30.4	30.2	30.2
$L_{2'}$	5.1	5.2	5.0
L_1	7.9	8.0	7.5
$L_{3'}$	17.2	17.2	16.7
L_1	27.8	27.5	27.6
L_3	28.5	28.2	28.2
X_1	8.0	8.1	7.8
X_4	14.3	14.4	13.7
X_1	25.9	25.5	26.2
X_4	33.9	33.8	33.3

[a]Reference 24.
[b]Tight binding (Ref. 4).

To determine the degree of convergence of our band structure, we performed a muffin-tin calculation using the potential given by Keown.[24] In Table III, we compare eigenvalues obtained from our calculation using 26 basis functions with the corresponding levels given by the first-principles APW calculation.[24] We have also included the tight-binding results of Chaney *et al.*[4] for their calculation with the same potential using 20 basis functions. The energies of the occupied states from the DVM calculation are converged to within 0.1 eV, assuming full convergence has been obtained in the APW calculation, while there is less accuracy in the conduction states. The more pronounced incomplete convergence of the tight-binding levels[4] given in the third column is probably a consequence of the reduced basis used in that computation.

The outstanding convergence problem common to the linear variational techniques is that concerning the finite basis set. In the tight-binding work of Chaney *et al.*,[4] an error estimate of 0.04 Ry due to basis truncation was reduced to 0.02 Ry by changing to a Gaussian basis, indicating that the restriction of atomic functions to Hartree-Fock form is an unnecessary one which restricts variational freedom for band-structure convergence. This may also explain the significantly larger discrepancies in their results for the indirect band gap, although their potential differed somewhat from that used here. In our calculation it was found that the carbon $3s$, $3p$ states contributed significantly to the eigenfunctions; however, the effect of including $3d$ orbitals in the basis was relatively small. It should be pointed out that the constituent STO functions were not combined into the form of

carbon free-atom Hartree-Fock orbitals, but were allowed to enter individually into the secular equation. By choosing the core STO's from existing optimized atomic HF minimal basis sets and supplementing with excited-state functions chosen to achieve desired bonding characteristics, we allow for relaxation effects of orbital expansion or contraction due to crystal formation. Since these atomic STO basis orbitals enter into the computation as nodeless functions, the formation of the nodal character of the crystal states is determined entirely by solution of the crystal secular equation. Thus, we allow variational freedom for the possibility of the existence of crystal states of various nodal structure of given symmetry (e.g., $3p$ as well as $2p$); the energy at which such Bloch eigenfunctions are formed is determined from solution of the secular equation. In this procedure, then, we obtain N eigenfunctions when we use N Bloch basis states formed of STO's, including all the core states as well as the valence and lower conduction states.

*Research sponsored by the U. S. Atomic Energy Commission under contract with the Union Carbide Corporation, by the Air Force Office of Scientific Research, and by the Advanced Research Projects Agency through the Northwestern University Materials Research Center.

†Alfred P. Sloan Research Fellow.

[1]F. Herman, R. L. Kortum, and C. D. Kuglin, Intern. J. Quantum Chem. 1S, 533 (1967). This article gives a good brief review of the development of band-theory treatments and experimental studies on diamond.

[2]L. Saravia and D. Brust, Phys. Rev. 170, 683 (1968).

[3]L. A. Hemstreet, Jr., C. Y. Fong, and M. L. Cohen, Phys. Rev. B 2, 2054 (1970).

[4]R. C. Chaney, C. C. Lin, and E. E. Lafon, Phys. Rev. B 2, 459 (1970).

[5]G. S. Painter and D. E. Ellis, Phys. Rev. B 1, 4747 (1970).

[6]J. C. Slater, Phys. Rev. 81, 385 (1951).

[7]D. E. Ellis and G. S. Painter, Phys. Rev. B 2, 2887 (1970).

[8]J. C. Slater, Solid State and Molecular Theory Group Semiannual Progress Report No. 71, Massachusetts Institute of Technology, 1969 (unpublished); J. C. Slater and J. H. Wood, Los Alamos Scientific Laboratory Report LA-DC-12001, 1970 (unpublished).

[9]*Methods in Computational Physics*, edited by B. Adler, S. Fernbach, and M. Rotenberg (Academic, New York, 1968), Vol. 8; *Computational Methods in Band Theory*, edited by P. M. Marcus, J. F. Janak, and A. R. Williams (Plenum, New York, 1971). These two references form an updated review of energy-band methods.

[10]D. J. Stukel, R. N. Euwema, T. C. Collins, F. Herman, and R. L. Kortum, Phys. Rev. 179, 740 (1969).

[11]P. D. DeCicco, Phys. Rev. 153, 931 (1967).

[12]L. F. Mattheiss, Phys. Rev. 181, 987 (1969).

[13]W. E. Rudge, Phys. Rev. 181, 1024 (1969).

[14]J. C. Slater and G. F. Koster, Phys. Rev. 94, 1498 (1954); G. Dresselhaus and M. S. Dresselhaus, *ibid.* 160, 649 (1967).

[15]C. Herring, Phys. Rev. 57, 1169 (1940); T. O. Woodruff, Solid State Phys. 4, 367 (1957), and references therein.

[16]F. Bloch, Z. Physik 52, 555 (1928).

[17]C. D. Clark, P. J. Dean, and P. V. Harris, Proc. Roy. Soc. (London) A277, 312 (1964).

[18]P. J. Dean and E. C. Lightowlers, Phys. Rev. 140, A352 (1965); E. O. Kane, *ibid.* 146, 558 (1966).

[19]R. A. Roberts and W. C. Walker, Phys. Rev. 161, 730 (1967).

[20]L. A. Schmid, Phys. Rev. 92, 1373 (1953).

[21]F. Herman and S. Skillman, *Atomic Structure Calculations* (Prentice-Hall, Englewood Cliffs, N.J., 1963).

[22]G. S. Painter, Intern. J. Quantum Chem. (to be published).

[23]R. Gaspar, Acta Phys. Hung. 3, 263 (1954); W. Kohn and L. J. Sham, Phys. Rev. 140, A1133 (1965).

[24]R. Keown, Phys. Rev. 150, 568 (1966).

[25]C. B. Haselgrove, Math. Comput. 15, 323 (1961); H. Conroy, J. Chem. Phys. 47, 5307 (1967); D. E. Ellis, Intern. J. Quantum Chem. 2, 35 (1968).

[26]H. Ehrenreich and M. H. Cohen, Phys. Rev. 115, 786 (1959).